Symmetrical MnO$_2$–Carbon Nanotube–Textile Nanostructures for Wearable Pseudocapacitors with High Mass Loading

Liangbing Hu,[†,||] Wei Chen,[‡,||] Xing Xie,[§] Nian Liu,[⊥] Yuan Yang,[†] Hui Wu,[†] Yan Yao,[†] Mauro Pasta,[†] Husam N. Alshareef,[‡] and Yi Cui[†,*]

[†]Department of Materials Science and Engineering, Stanford University, Stanford, California 94305, United States, [‡]Materials Science and Engineering, King Abdullah University of Science and Technology (KAUST), Thuwal, Saudi Arabia, and [§]Department of Civil and Environmental Engineering and [⊥]Department of Chemistry, Stanford University, Stanford, California 94305, United States. [||]These authors contributed equally to this work.

Power density, energy density, and cycling performance are key parameters for energy storage devices. Typically, batteries have high energy densities, low power densities, and limited cycle lives. Ultracapacitors based on electrochemical double-layer (DL) mechanisms have higher power densities but lower energy densities compared to batteries.[1−6] For certain applications, such as large-scale energy storage connected with solar cell and wind energy, the power density needs to be high and the device needs to respond quickly enough to the power fluctuations. There are typically two routes to accomplish this task: increase the energy density of ultracapacitors or increase the power density of batteries. To increase the energy density of an ultracapacitor, increasing the voltage range is an effective approach, and recently, Izadi-Najafabadi *et al.* demonstrated 4 V ultracapacitors based on single-walled CNT.[7] Further improvement will be limited by the electrolyte stability. Using nanostructured battery electrodes has largely improved the power densities of battery devices.[8−10] However, the device performance and the cost still do not meet the requirements for large-scale grid applications. Pseudocapacitors are based on the redox reactions of electrodes such as conductive polymers or transition metal oxides.[11] These pseudocapacitors typically have higher energy densities than ultracapacitors and higher power densities than batteries. MnO$_2$ is a low-cost material with a large theoretical capacity, two desirable traits for pseudocapacitor materials.[12−18] However, many challenges exist, which include its low electronic conductivity,

ABSTRACT While MnO$_2$ is a promising material for pseudocapacitor applications due to its high specific capacity and low cost, MnO$_2$ electrodes suffer from their low electrical and ionic conductivities. In this article, we report a structure where MnO$_2$ nanoflowers were conformally electrodeposited onto carbon nanotube (CNT)-enabled conductive textile fibers. Such nanostructures effectively decrease the ion diffusion and charge transport resistance in the electrode. For a given areal mass loading, the thickness of MnO$_2$ on conductive textile fibers is much smaller than that on a flat metal substrate. Such a porous structure also allows a large mass loading, up to 8.3 mg/cm^2, which leads to a high areal capacitance of 2.8 F/cm^2 at a scan rate of 0.05 mV/s. Full cells were demonstrated, where the MnO$_2$–CNT–textile was used as a positive electrode, reduced MnO$_2$–CNT–textile as a negative electrode, and 0.5 M Na$_2$SO$_4$ in water as the electrolyte. The resulting pseudocapacitor shows promising results as a low-cost energy storage solution and an attractive wearable power.

KEYWORDS: MnO$_2$ · carbon nanotube · textile · pseudocapacitor · large-scale · wearable device

low ion diffusion constant, Mn dissolution into electrolyte, and others.[12] Various nanostructures have been reported to overcome the problems of low electrical and ionic conductivities. MnO$_2$ nanomaterial-based composites with conductive additives such as carbon nanotubes (CNTs) or graphene have been widely studied.[15,19−22] *In situ* grown MnO$_2$ on CNTs or graphene has also been demonstrated. Various shapes of MnO$_2$ nanostructures have also been developed such as MnO$_2$ nanorods and nanotubes.[23] For example, Hou *et al.* recently developed a rational design of MnO$_2$ wrapped with conductive PEDOT to effectively improve the usage of MnO$_2$ and the overall device performance.[24] Lee *et al.* used layer-by-layer deposition of MnO$_2$ with carbon nanotubes electrically connecting the rather insulating electrode materials together.[25] Lang *et al.*
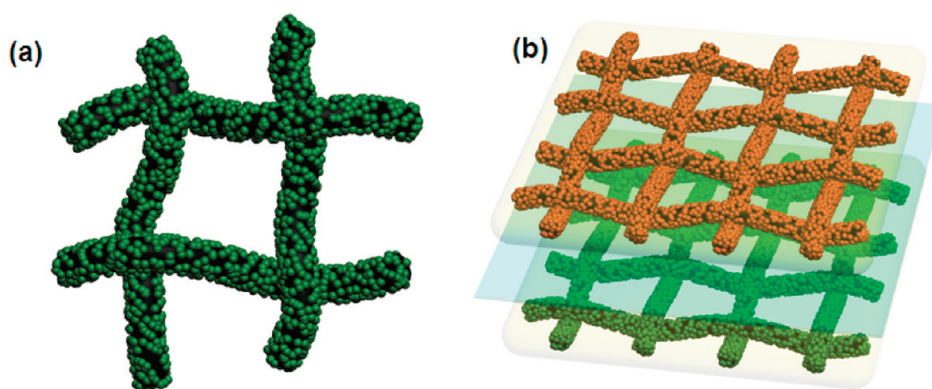
Figure 1. (a) Schematic of conformal coating of MnO_2 on CNT-wrapped polyester fibers. Black, CNT−polyester fibers; green, MnO_2 nanoflowers. (b) Schematic of pseudocapacitor based on MnO_2−CNT−textile. The positive electrode (bottom) is MnO_2, the negative electrode (top) is reduced MnO_2, and the electrolyte is 0.5 M Na_2SO_4 in water at pH 10.

developed a nanoporous metal−oxide hybrid structure which results in a specific capacitance of ∼1145 F/g, close to the theoretical value for MnO_2.[26] However, the fabrication process for these MnO_2 nanostructures is not scalable for large-scale energy storage applications.

Recently, we demonstrated energy storage devices based on conductive paper or textile with CNTs.[27,28] Kang et al. demonstrated a promising candidate for a flexible and low-cost energy storage device based on MnO_2/CNT/paper structure.[29] In this study, we report a new nanostructure based on a conductive CNT−textile fiber network, which provides an effective three-dimensional (3D) framework for the electrodeposition of nanoscale MnO_2. Such a 3D network allows for a large mass loading of MnO_2 without any mechanical peeling problems. The processes for fabricating conductive textiles and depositing MnO_2 are scalable. The MnO_2 shows much stronger binding with CNT−textile fibers than metal substrates, which is beneficial for stable cycling performance. A high specific capacitance of 410 F/g is achieved, which decreases with film thickness and faster charging−discharging rates. Large areal capacitances up to 2.8 F/cm^2 are achieved, which is much higher than values for other MnO_2 nanostructures demonstrated in the literature (typically 0.01−0.1 F/cm^2)[19,25] and is comparable to the best performance (1−7 F/cm^2) demonstrated recently.[30,31] Full cells based on MnO_2−CNT−textile nanostructures were demonstrated with 0.5 M Na_2SO_4 in water as the electrolyte, which could be potentially useful for future large-scale stationary energy storage applications.

RESULTS AND DISCUSSION

Conductive textiles were fabricated with a conformal coating of CNTs on the surface of polyester fibers.[28] Due to the high flexibility of CNTs and the large van der Waals forces between CNTs and polyester fibers, an excellent overcoating is observed as shown in our previous work.[28] Figure 1a illustrates the structure of the pseudocapacitor electrode, where MnO_2 is conformally electrodeposited onto the highly conductive polyester fibers. CNTs have −COOH groups on the surface that promote the nucleation of MnO_2 and bonding with the conductive textile. Figure 1b shows the final device structure with the MnO_2−CNT−textile as a positive electrode, reduced MnO_2−CNT−textile (R-MnO_2−CNT−textile) as a negative electrode, and 0.5 M Na_2SO_4 in water at pH 10 as the electrolyte. The advantages of such a pseudocapacitor are as follows: (1) the conductive textile is much lighter than metal foil as a current collector, which reduces the total weight of the pseudocapacitor; (2) the highly macroporous structure of the textiles allows for a large mass loading of MnO_2, much larger than that on flat metal substrate on the same projection area; (3) the strong binding between MnO_2 and CNT-coated polyester fibers is beneficial for achieving stable performance; (4) the material and the process could lead to low-cost pseudocapacitors. Although the cost of CNTs is relatively high, the areal mass loading of CNTs is low (less than 0.2 mg/cm^2). Also, the cost of CNTs is projected to drop in the future with further commercialization efforts. Other conductive nanomaterials with potential low costs such as graphene and conductive polymers can replace CNTs in our pseudocapacitors.

After washing away the surfactant thoroughly with deionized (DI) water, the conductive textile is hydrophobic. To ensure conformal coating of MnO_2 over the entire textile surface including the fibers inside, textiles are soaked in 4 M HNO_3 for 4 h to generate −COOH groups on CNTs, taken out, and dried in air for 1 h.[32] The textile is cut with a size of 1 cm by 3 cm, where 1 cm by 1 cm is immersed into aqueous solution with 100 mM Na_2SO_4 and 10 mM $MnSO_4$. MnO_2 is electrodeposited onto the conductive textile with a three-electrode setup, where a conductive textile with a sheet resistance of ∼10 Ω/□ is used as the working electrode, platinum (Pt) as the counter electrode, and Ag/AgCl as the reference electrode. A small piece of Pt is used to connect the textile and the alligator clip to avoid side reactions. Impedance spectra in the frequency range of 0.1 Hz to 100 kHz are recorded
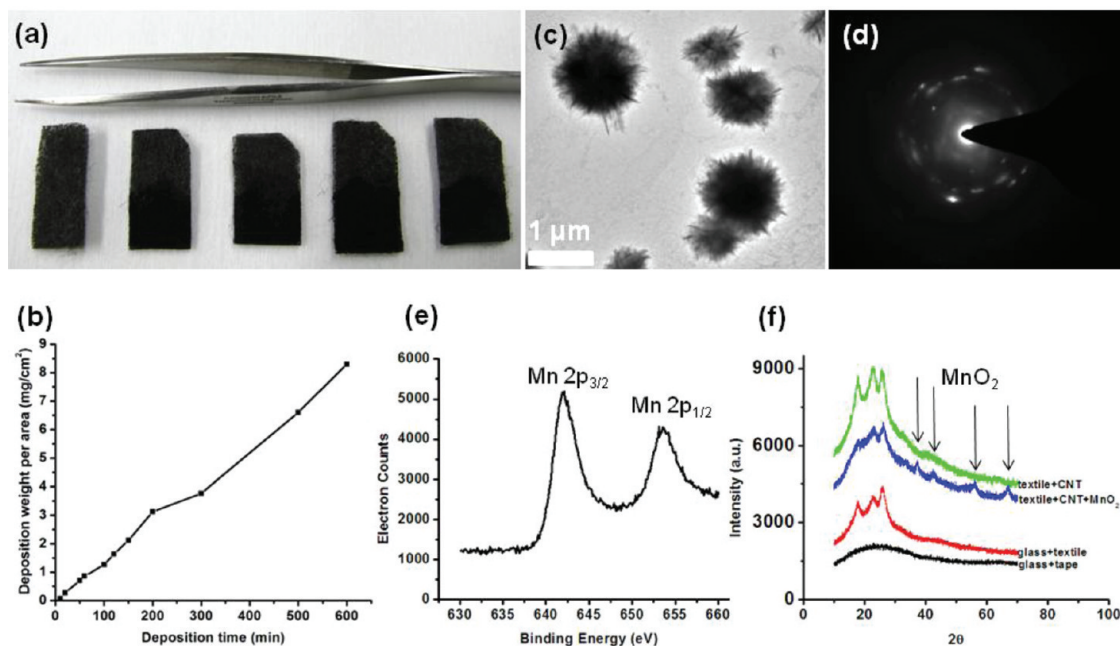
Figure 2. (a) MnO$_2$ deposited on conductive textiles with different areal masses. The MnO$_2$ mass increases from left to right (0.06, 0.3, 0.8, 2.1, 3.8 mg/cm^2). (b) MnO$_2$ weight *vs* deposition time. (c) TEM image of MnO$_2$ nanoflowers by electrodeposition. (d) TEM diffraction pattern of MnO$_2$ nanoflowers. (e) XPS of MnO$_2$−CNT−textile. (f) XRD patterns of textile, CNT−textile, and MnO$_2$−CNT−textile.

before the electrodeposition to check the connections. Typical resistance at high frequency (∼100 kHz) is ∼20 Ω. The MnO$_2$ is electrodeposited with a galvanostatic technique by applying a small current, 500 μA, to ensure a conformal coating of MnO$_2$.

Figure 2a shows the conductive textiles after MnO$_2$ deposition. The bottom surface becomes darker as the deposition time increases, which indicates more materials were deposited. Figure 2b shows the mass loading *versus* deposition time. Due to the highly porous structure of the textile, a larger mass loading of MnO$_2$ is achieved by increasing the deposition time; 8.3 mg/cm^2 of MnO$_2$ is readily achieved, where the textile structure is still highly porous. Pseudocapacitors based on MnO$_2$ typically have small mass densities (<0.5 mg/cm^2) due to its low proton diffusion constant (∼10^{-13} cm^2/s) and low electrical conductivity (∼10^{-5} S/cm).[12] We found that the MnO$_2$ nanoflowers are polycrystalline, which is consistent with the literature (Figure 2c,d). The strong signals at 642 and 653 eV in the X-ray photoelectron spectroscopy (XPS) in Figure 2e correspond to the binding energies of Mn 2p$_{3/2}$ and 2p$_{1/2}$, respectively.[25] The well-resolved peak at 37.1° *etc.* in the X-ray diffraction (XRD) pattern marked by the arrows (Figure 2f) are attributed to MnO$_2$,[19] and the other peaks are from textiles or CNTs.[23]

Figure 3 shows SEM images of the MnO$_2$ deposited on conductive textile with different electrodeposition times. MnO$_2$ forms nanoflower structures, which is consistent with previous studies. MnO$_2$ nanoflowers and CNTs can be clearly identified (Figure 3a,b). As the deposition time increases, the sizes of the nanoflowers

increase until a continuous, thick MnO$_2$ layer is formed on the textile fibers (Figure 3c,d). Even for a large mass loading, ∼8.3 mg/cm^2, the 3D textile fiber structure is still maintained without merging into a film. Such a highly porous structure with a large mass loading is excellent for pseudocapacitor applications. During the experiment, we found that the treatment of the conductive textile is crucial for achieving such a uniform coating. The conductive textile was washed with HNO$_3$ to remove surfactants and generated −COOH groups.[32] The washed textile was dried in air for an hour before MnO$_2$ deposition. A longer drying time in air makes the conductive textile highly hydrophobic, which prohibits electrolyte penetration and the deposition of MnO$_2$ inside the structure. A shorter drying time leads to a highly hydrophilic textile, which allows the water to climb along the fibers and cause corrosion on the metal connector during the electrodeposition process.

Impedance of the half cells with a three-electrode setup is tested over a frequency range of 100 kHz to 0.1 Hz with MnO$_2$−CNT−textile as the working electrode, Pt as the counter electrode, and Ag/AgCl as the reference electrode (Figure 4a). Na$_2$SO$_4$ (0.5 M) in DI water was used as the electrolyte. Impedance of flat Pt without MnO$_2$ deposition was tested as a control experiment, which reflects the contribution from the electrolyte (∼7 Ω) between the working electrode and the counter electrode in our setup. The impedance at a high frequency (100 kHz) for MnO$_2$−CNT−textile reflects the combination of electrolyte resistance and textile electrode resistance. For example, the
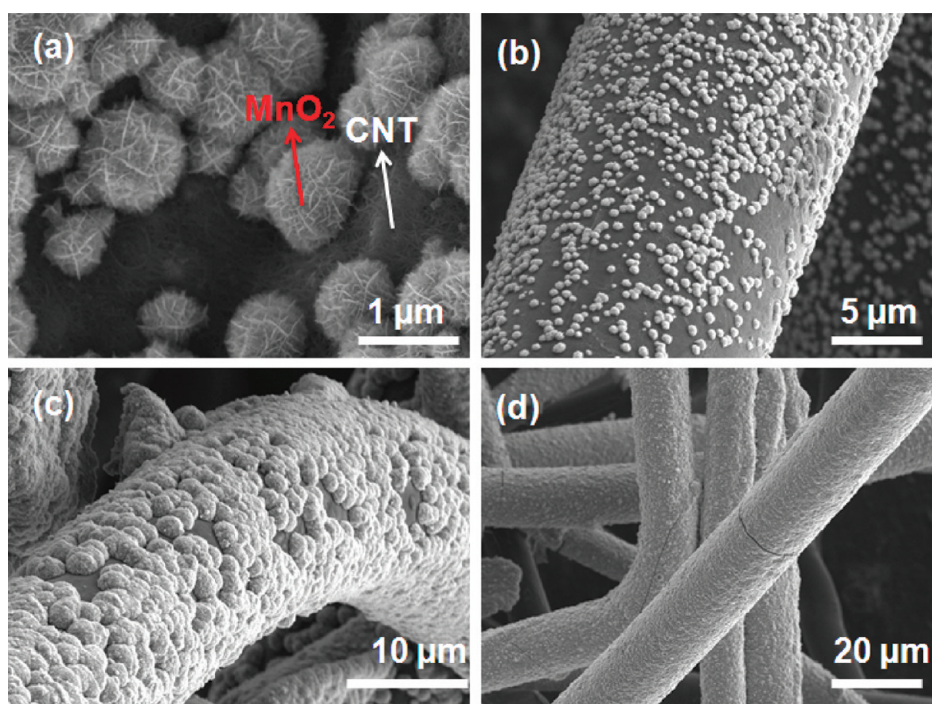
Figure 3. (a,b) SEM of MnO$_2$−CNT−textile after a 10 min deposition. (c,d) SEM of MnO$_2$−CNT−textile after 120 and 300 min depositions, respectively.
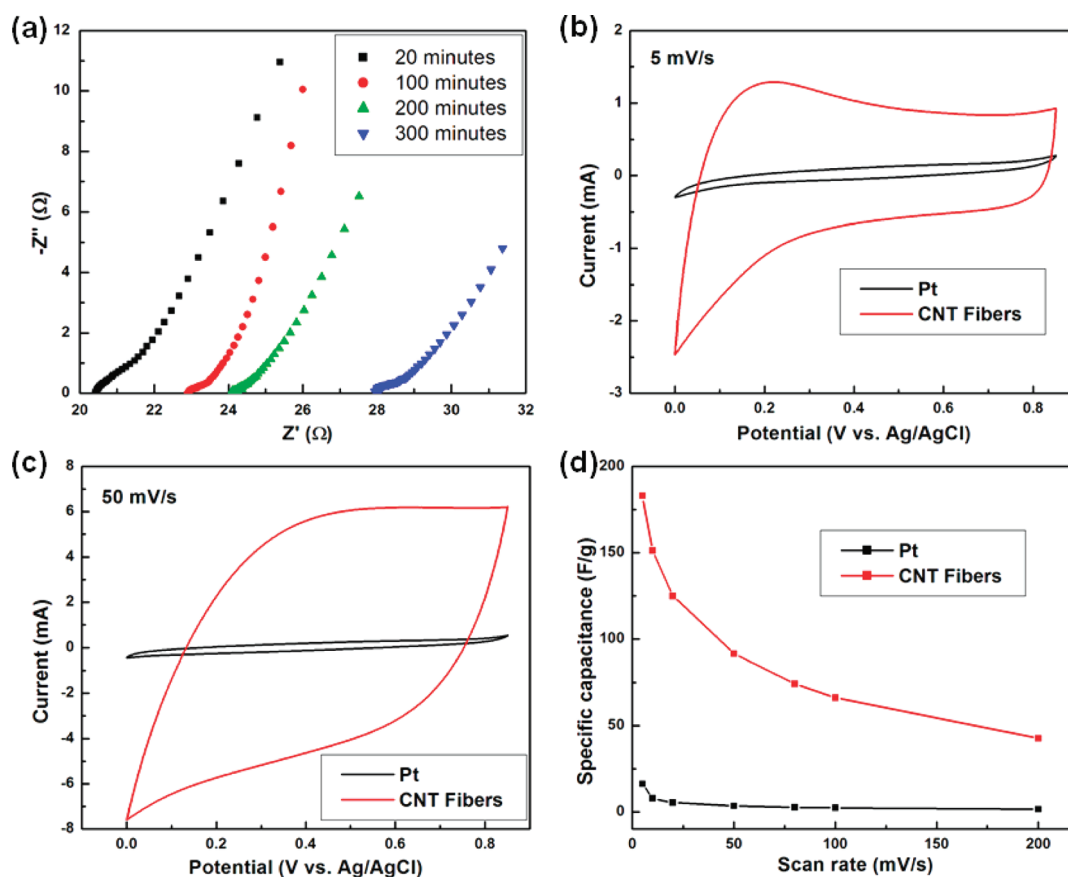

Figure 4. (a) Impedance of MnO$_2$−CNT−textiles with different MnO$_2$ deposition times. The frequency range is 100 kHz to 0.1 Hz. (b,c) CV scan comparison of MnO$_2$−CNT−textile and MnO$_2$−Pt at scan rates of 5 and 50 mV/s, respectively. (d) Specific capacitance comparison between MnO$_2$−CNT−textile and MnO$_2$−Pt. The mass density of MnO$_2$ for both substrates is 0.8 mg/cm^2.
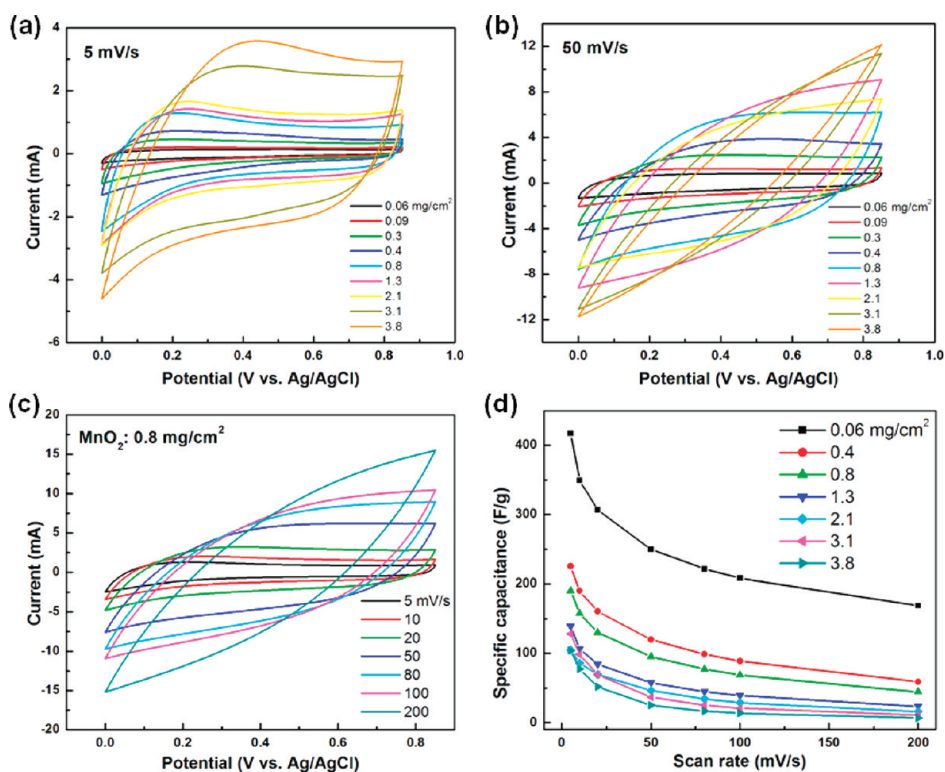
Figure 5. (a,b) CV scan of MnO_2−CNT−textile with different areal mass densities for MnO_2. The scan rate is (a) 5 mV/s and (b) 50 mV/s. (c) CV of MnO_2−CNT−textile with different scan rates. The areal mass for MnO_2 is 0.8 mg/cm^2. (d) Specific capacitance *vs* scan rate for samples with different areal mass densities for MnO_2.

total resistance of MnO_2−CNT−textile with a 20 min deposition at 100 kHz is 20.4 Ω (Figure 4a), and 13.4 Ω is contributed by the textile electrode and 7 Ω by the electrolyte.

To illustrate the advantages of the 3D porous textile electrode-based pseudocapacitors, a comparison study of MnO_2 pseudocapacitor with a flat Pt substrate was conducted. The MnO_2 deposition time is 60 min for both the Pt substrate and conductive textile. The areal mass is approximately 0.8 mg/cm^2. The coating is uniform on both sides of the Pt plate immersed into the electrolyte solution. After drying in air, the MnO_2 film on Pt is fragile and easily cracks into pieces. Electrochemical performance was evaluated for MnO_2−Pt and MnO_2−CNT−textile, where MnO_2−Pt is not dried to avoid cracking. The voltage range is chosen according to the Pourbaix diagram of MnO_2. Figure 4b, c shows the CV comparisons between MnO_2−Pt and MnO_2−CNT−textile at scan rates of 5 and 50 mV/s, respectively. With the same mass density of 0.8 mg/cm^2, the capacitance for the MnO_2−CNT−textile is much higher than that for MnO_2−Pt. As shown in Figure 4d, a specific capacitance of 185 F/g is achieved for the CNT−textile-based device, while only 18 F/g for the Pt-based device. The specific capacitance is based on the mass of MnO_2 on the substrates. This 10-fold difference in specific capacitance with respect to the mass of MnO_2 at the same scan rate must be due to the kinetics of ions and electrons in the electrode

materials. For the same mass loading, the thickness of MnO_2 on textile fibers is much smaller than that on the Pt substrate, which largely facilitates the ion and electron transport in the electrode materials. As the scan rate increases, the specific capacitance decreases for both substrates. This study clearly illustrates that the 3D CNT−textile fiber is better than a flat metal current collector for pseudocapacitor applications.

To achieve the highest specific capacitance with respect to MnO_2 mass, the thickness needs to be infinitely small, and the scan rate needs to be infinitely slow to enhance the transport of electrons and ions in the electrode materials. However, high-power performance at the device level depends on the total mass, which includes all of the components in a device (electrolyte, current collectors, electrodes, separator, packaging, *etc.*). Therefore, the optimization of MnO_2 mass percentage with respect to the total mass is important. We have carried out a detailed study of changing the mass loading and the scan rate in a large range to identify a trend, which will be useful for designing practical pseudocapacitors based on conductive textiles. First, we performed CV scans of a MnO_2−CNT−textile with a large range of MnO_2 deposition times on conductive textile (from 5 to 600 min). The MnO_2 mass varies from 60 μg to 8.3 mg per cm^2 accordingly. The electrochemical performance of MnO_2−CNT−textiles was tested with two different scan rates (5 and 50 mV/s). As the MnO_2
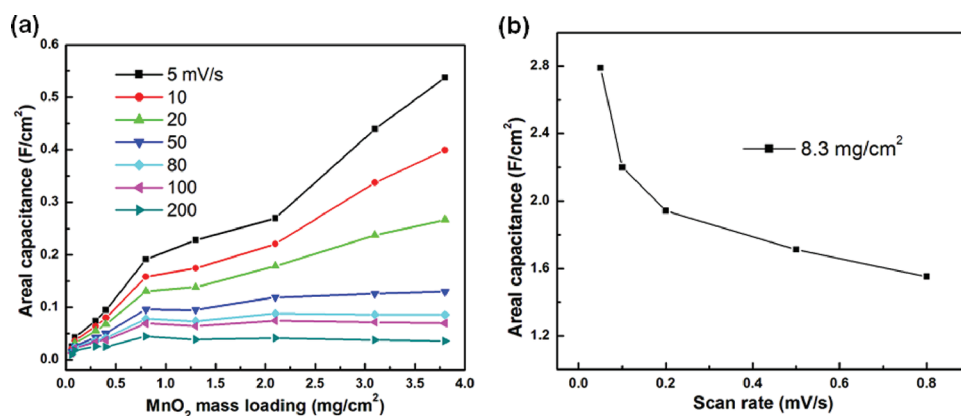
Figure 6. (a) Areal capacitance of MnO_2-CNT-textile *vs* MnO_2 mass loading. (b) Areal capacitance *vs* scan rate for a sample with 8.3 mg/cm^2 MnO_2.

mass increases, the total capacitance increases at the same scan rate, as indicated by the increases of the current (Figure 5a,b). As the scan rate increases from 5 to 50 mV/s, the overpotentials lead to large resistance and the RC time constant causes the curves to deviate from those of an ideal capacitor (Figure 5b). Second, we varied the scan rate from 5 to 200 mV/s for MnO_2-CNT$-$textiles. The CV scan of the 0.8 mg/cm^2 sample is shown in Figure 5c. As the scan rate increases, the peak current increases but the shape deviates from that of an ideal capacitor. The specific capacitance with respect to the electrode mass *versus* the scan rates is shown in Figure 5d. As the scan rate increases, the capacitance decreases dramatically for MnO_2-CNT$-$textile. The highest specific capacitance is 410 F/g for the sample with a mass density of 0.06 mg/cm^2 at a scan rage of 5 mV/s. As the thickness increases, the specific capacitance decreases due to the kinetics of ion transport in MnO_2 with its low ion diffusion constants. The low electrical conductivity and the low diffusion constant limit the pseudocapacitor performance.

It is worthwhile to point out that the mass loading per area is important for battery or pseudocapacitor devices. It is a considered good practice to report the values of the electrode mass.[33] The areal capacitance *versus* MnO_2 with different mass loadings is plotted in Figure 6a. At a fixed rate of 200 mV/s, the areal capacitance increases with the mass until a saturation value is reached at a deposition time of approximately 60 min. At this fixed scan rate, the capacitance increases with MnO_2 thickness or mass until a critical value is reached. The critical MnO_2 thickness should be close to the Na$^+$ diffusion length at this rate. The critical mass loading at a fixed scan rate is helpful for device designs. As the scan rate decreases, the ion diffusion length in MnO_2 increases and more of electrode material contributes to the energy storage. For example, at 20 mV/s, the critical areal mass of MnO_2 is 3.8 mg/cm^2 (300 min). For 5 mV/s, no saturation was observed in the range of measurement and all of the MnO_2

contributes to the energy storage. The highly porous structures of conductive textiles allow for the demonstration of pseudocapacitors with extremely high areal capacitances. Figure 6b shows areal capacitance *versus* scan rate for MnO_2-CNT$-$textile samples with a mass loading of 8.3 mg/cm^2. Such high areal mass loadings are not reported in the literature, and 2.8 F/cm^2 at slow a scan rate of 0.05 mV/$_S$ is demonstrated.

According to the Pourbaix diagram, reduced MnO_2 (R-MnO_2) at pH 10 has a lower potential than that of MnO_2. As outlined in Figure 1b, R-MnO_2-CNT$-$textile with the same electrode morphology (*i.e.*, R-MnO_2 on conductive textile fibers) is used as the negative electrode in the aqueous pseudocapacitors. When a negative bias with current density of -500 μA/cm^2 is applied on a MnO_2-CNT$-$textile, the following reaction happens: $MnO_2 + xNa^+ + xe^- \rightarrow MnOONa_x$. Figure 7a,b shows the morphology of R-MnO_2-CNT$-$textile with nanoflower-like structures which are similar to those of the MnO_2-CNT$-$textile. Here, the deposition time for the MnO_2-CNT$-$textile is 60 min. TEM images show that the R-MnO_2 nanoflower is polycrystalline with a diameter of $\sim$0.5 μm (Figure 7c). XPS shows clearly the presence of Mn ions and Na$^+$ (Figure 7d). The strong signals at 642 and 653 eV are located in close proximity to those for MnO_2 (Figure 2e). Because of the overlapping of the XPS signals for Mn^{2+}, Mn^{3+}, and Mn^{4+} around 642 and 653 eV, it is difficult to tell the valence value of the R-MnO_2-CNT$-$textile. The separation of peak energies between the two peaks of the Mn 3s components has been used to identify the oxidation state of Mn, where the separations are $\sim$4.8 and $\sim$5.4 eV for Mn^{4+} and Mn^{3+}, respectively.[34] We have not been able to conclude the oxidation states from the energy separation of the Mn 3s components due to the strong background signals.

The electrochemical performance of the R-MnO_2-CNT$-$textile was carried out with CV scan in the voltage range of -0.2 to 0.2 V with respect to Ag/AgCl. No side reactions were observed in the CV scans (Figure 8a). The full cells are assembled in the configuration of pouch cells, with the MnO_2-CNT$-$textile as the positive
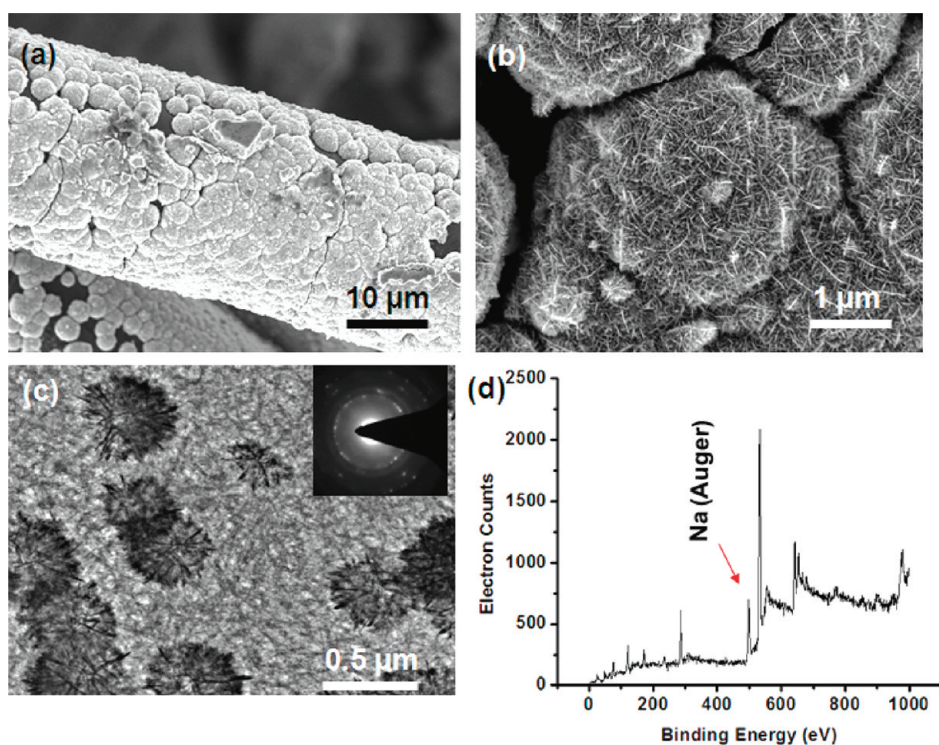
Figure 7. (a,b) SEM images of R-MnO$_2$−CNT−textile at different magnifications. (c) Nanoflower structure of reduced MnO$_2$. The inset shows the TEM diffraction pattern. (d) XPS of R-MnO$_2$.
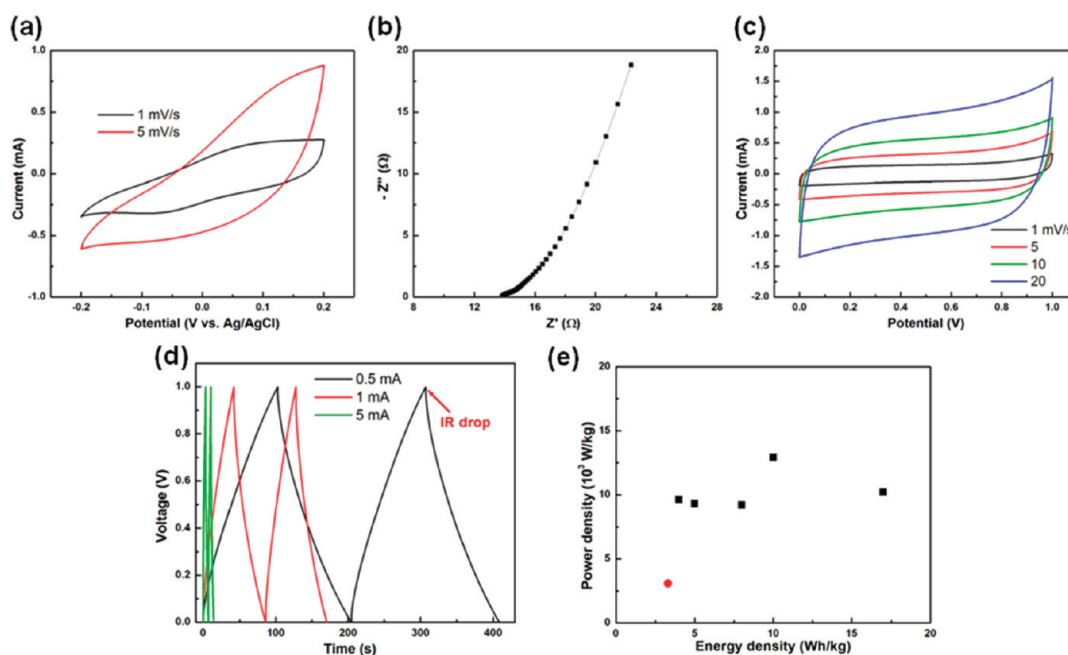

Figure 8. (a) CV scan of R-MnO$_2$−CNT−textile at two different scan rates between −0.2 and 0.2 V. (b) Impedance of a pouch cell with MnO$_2$−CNT−textile as the positive electrode and R-MnO$_2$−CNT−textile as the negative electrode. (c) CV of the pouch full cell at different scan rates in the voltage range of 0−1.0 V. (d) Galvanostatic cycling at different rates. (e) Ragone plot of the full cell at different current densities.

electrode, R-MnO$_2$−CNT−textile as the negative electrode, and Whatman filter paper as the separator. The impedance of the full cell is shown in Figure 8b, with a resistance of ∼13.8 Ω at a high frequency of 100 kHz. The impedance is relatively higher compared with previous values in the literature for a MnO$_2$ supercapacitor, which is due to the resistance of the conductive textile. Since MnO$_2$ is stable between 0 and 0.85 V and R-MnO$_2$ is stable between −0.2 and 0.2 V, the assembled cell is cycled in 0−1.0 V. Note that the potential may drift during the
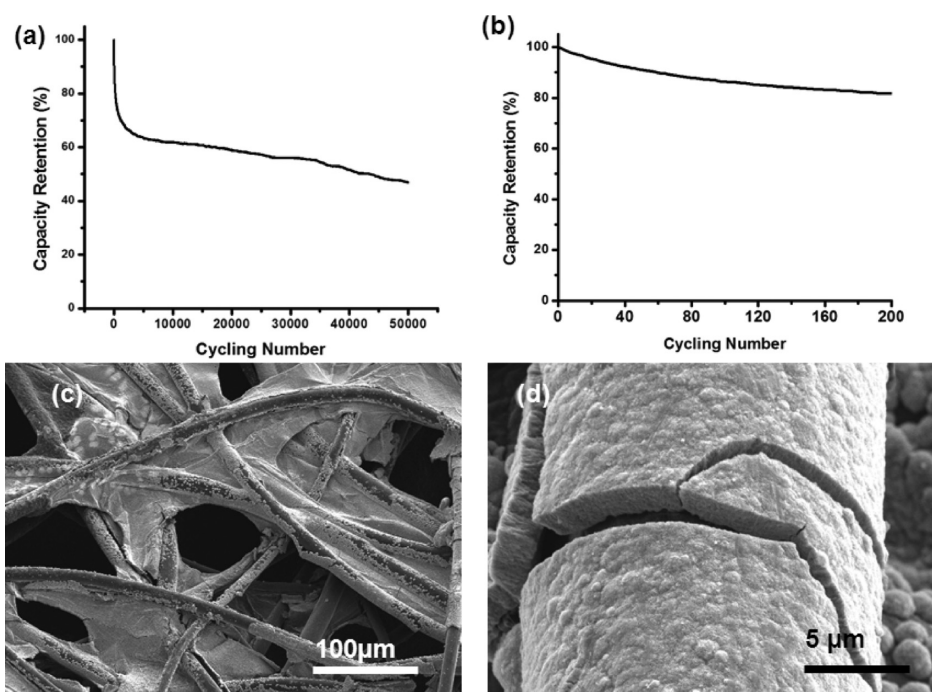
Figure 9. (a,b) Capacity retention of a full cell. (c,d) SEM images of MnO_2—CNT—textile after 50 000 cycles.

test which has a negative effect for the cycling performance. The CV scan is performed for the assembled pseudocapacitors at different scan rates (*i.e.*, 1, 5, 10, and 20 mV/s; Figure 8c). The rectangular shapes of the CV scans indicate a strong capacitive behavior. Galvanostatic cycling was also performed with different current densities. Figure 8d shows the cycling with current densities of 0.5, 1, and 5 mA/cm^2. The Coulombic efficiencies are 97.7, 98.2, and 99.2% for those currents, respectively. The internal resistance (IR) drop is used to calculate the power and energy density. The resistance from the IR drop is 12.1 Ω at 200 μA/cm^2, 15.5 Ω at 500 μA/cm^2, 16.4 Ω at 1 mA/cm^2, and 16.8 Ω at 2 mA/cm^2, which are close to the values from the impedance measurements (Figure 8b). The energy density and power density with respect to MnO_2 are calculated using $E = 0.5$ CV^2/M and $P = 0.25$ $V^2/(RM)$, where C is the capacitance from Figure 8d, $V = 1.0$ V, R is the resistance from the IR drop, and M is the total mass of active materials on both electrodes. The data for the MnO_2—CNT—textile with a 60 min deposition time with different current rates are shown in Figure 8e. A power density of $\sim$13 000 W/kg and an energy density $\sim$5—20 Wh/kg are achieved. For comparison, the red dot represents the performance from the literature where MnO_2 was used as the active material in both electrodes.[35] The improvement is likely due to the usage of the 3D textile conductors which facilitates the electronic and ionic transport in the device. The performance can be further improved with use of asymmetrical structure, such as In_2O_3 electrodeposited on CNT—textile as a negative electrode.[12,36]

Pseudocapacitors based on conductive textiles with high areal mass loadings through a scalable electrodeposition method are promising for large-scale energy storage. Cycling performance is critical for this application. There are various possible causes for the failure of MnO_2-based pseudocapacitors under long cycling: (1) mechanical expansion upon ion insertion; (2) delamination of electrode materials from substrates; (3) unbalanced capacity on the two electrodes which causes instability of the electrode potentials; (4) dissolution of Mn into the electrolyte.[12,13] The pouch cell (the MnO_2—CNT—textile was used as a positive electrode, reduced MnO_2—CNT—textile as a negative electrode, and 0.5 M Na_2SO_4 in water as the electrolyte) was cycled between 0 and 1 V for 50 000 cycles (Figure 9a); 80% capacity was retained after the first 200 cycles (Figure 9b). Note that the areal mass of MnO_2 for the cell is 0.8 mg/cm^2, which is higher than those in the literature.[25] The cycling performance is expected to be improved dramatically as the areal mass loading decreases. As the mass density decreases, the MnO_2 decreases, which will help release the mechanical strain induced by the ion diffusion into the electrode; 60% capacity was retained after 10 000 cycles and 50% for 50 000 cycles (Figure 9a). The poor cycling performance is not fully understood yet. Possible solutions could include the following: (1) at a given areal mass density, using textile fibers with smaller diameters which could decrease the MnO_2 thickness on conductive fibers to mitigate the mechanical strain; (2) using electrolyte with smaller ion sizes such as Li_2SO_4 with Li^+; (3) forming porous structures of MnO_2 on textile fibers. After 50 000 cycles, the cells

were dissembled to investigate the electrode morphology. Figure 9c,d show the SEM of MnO_2–CNT–textile. The flower structure is maintained, and MnO_2 is still conformally coated on the textile fibers. However, occasional cracks were observed in the electrodes, which may cause some electrical disconnection between the MnO_2 and the conductive fibers. As in Li-ion batteries, volume expansion also occurs in MnO_2-based pseudocapacitors with Na_2SO_4 as the electrolyte. Na^+ intercalation into MnO_2 structures tends to cause structure breaks and device failure.[37] *In situ* studies using X-ray spectroscopy are ongoing to study the volume expansion of MnO_2–CNT–textile during the charge and discharge process.

CONCLUSION

In conclusion, a nanostructured MnO_2–CNT–textile has been studied for pseudocapacitor applications in detail. Such MnO_2 nanostructures have specific capacitances 10 times higher than those on flat metal substrates. A high specific capacitance of 410 F/g and a high areal capacitance of 2.8 F/cm^2 are achieved. We studied the rate and thickness dependence of the pseudocapacitance of MnO_2–CNT–textile nanostructures. Such pseudocapacitors can be realized by low-cost materials and scalable processing and are promising for large-scale wearable energy storage.

EXPERIMENTAL SECTION

Chemicals. All chemicals were purchased from Sigma Aldrich, unless otherwise specified, and were used without further purification.

Preparation of MnO_2–CNT–Textile Electrodes. Single-walled carbon nanotubes (Carbon Solution Inc.) and sodium dodecylbenzenesulfonate (SDBS) were dispersed in DI water at a concentration of 1.6 and 10 mg/mL, respectively. After 10 min bath sonication (Branson 2510), the dispersion was ultrasonicated for 30 min using a probe sonicator (VC505, 200 W, Sonics Inc.). Upon preparation of the as-prepared CNT-ink, a piece of cotton sheet (Cloud 9 dream fleece, Wal-Mart) was dipped into the CNT-ink and immediately removed. After drying in an electrical oven at 120 °C for 10 min, the cotton sheet was washed by an abundant amount of water in order to get rid of the surfactant. The dipping and drying process was repeated three times to increase the CNT loading on the textile. The CNT–textile was subsequently dipped into 4 M nitric acid solution for 4 h and was cut into many small pieces with sizes of 1 cm by 3 cm after drying. In order to electrodeposit MnO_2 on the CNT–textile, an aqueous solution consisting of 100 mM Na_2SO_4 and 10 mM $MnSO_4$ was first prepared. The electrodeposition of MnO_2 nanoflower particles was carried out by a three-electrode configuration, where the CNT–textile (1 cm by 1 cm) immersed into the solution was used as working electrode, Ag/AgCl as reference electrode, and a piece of Pt foil as counter electrode. A constant current of 500 μA was applied over a wide range of time scales: from 5 to 600 min. After electrodeposition, the textile was washed by DI water to remove the excessive electrolyte and dried in a vacuum oven at 60 °C for 1 h. The mass loading of CNT and MnO_2 on the textile was measured by a microbalance before and after the materials loading.

Electrochemical Measurement. All electrochemical measurements were conducted by using VMP3 multichannel electrochemical workstation (Biologic, Inc.) at room temperature. In the half cell tests, a three-electrode configuration was used to measure the cyclic voltammetry, constant current charge–discharge behavior, and electrochemical impedance spectroscopy, where MnO_2–CNT–textile was used as working electrode, Ag/AgCl as reference electrode, and a piece of Pt as counter electrode. In the full cell tests, a two-electrode coin cell (CR2032, MTI) was assembled to measure the device performances. The MnO_2–CNT–textile (area of 1 cm by 1 cm) and reduced MnO_2–CNT–textile (area of 1 cm by 1 cm) were used as positive and negative electrodes, respectively. The electrode served as current collector as well as conductive electrode. The electrolyte used in all of the measurements was 0.5 M Na_2SO_4 aqueous solution at pH 10.

REFERENCES AND NOTES

1. Conway, B. E. Transition from "Supercapacitor" to "Battery" Behavior in Electrochemical Energy Storage. *J. Electrochem. Soc.* **1991**, *138*, 1539–1548.
2. Zhang, L. L.; Zhao, X. S. Carbon-Based Materials as Supercapacitor Electrodes. *Chem. Soc. Rev.* **2009**, *38*, 2520–2531.
3. Simon, P.; Gogotsi, Y. Materials for Electrochemical Capacitors. *Nat. Mater.* **2008**, *7*, 845–854.
4. Niu, Z.; Zhou, W.; Chen, J.; Feng, G.; Li, H.; Ma, W.; Li, J.; Dong, H.; Ren, Y.; Zhao, D.; Xie, S. Compact-Designed Supercapacitors Using Free-Standing Single-Walled Carbon Nanotube Films. *Energy Environ. Sci.* **2011**, *4*, 1440–1446.
5. Lota, G.; Fic, K.; Frackowiak, E. Carbon Nanotubes and Their Composites in Electrochemical Applications. *Energy Environ. Sci.* **2011**, *4*, 1592–1605.
6. Hall, P. J.; Mirzaeian, M.; Fletcher, S. I.; Sillars, F. B.; Rennie, A. J. R.; Shitta-Bey, G. O.; Wilson, G.; Cruden, A.; Carter, R. Energy Storage in Electrochemical Capacitors: Designing Functional Materials To Improve Performance. *Energy Environ. Sci.* **2010**, *3*, 1238–1251.
7. Izadi-Najafabadi, A.; Yasuda, S.; Kobashi, K.; Yamada, T.; Futaba, D. N.; Hatori, H.; Yumura, M.; Iijima, S.; Hata, K. Extracting the Full Potential of Single-Walled Carbon Nanotubes as Durable Supercapacitor Electrodes Operable at 4 V with High Power and Energy Density. *Adv. Mater.* **2010**, *22*, E235–E241.
8. Zhang, H. G.; Yu, X. D.; Braun, P. V. Three-Dimensional Bicontinuous Ultrafast-Charge and -Discharge Bulk Battery Electrodes. *Nat. Nanotechnol.* **2011**, *6*, 277–281.
9. Kang, K. S.; Meng, Y. S.; Breger, J.; Grey, C. P.; Ceder, G. Electrodes with High Power and High Capacity for Rechargeable Lithium Batteries. *Science* **2006**, *311*, 977–980.
10. Kang, B.; Ceder, G. Battery Materials for Ultrafast Charging and Discharging. *Nature* **2009**, *458*, 190–193.
11. Conway, B. W. *Electrochemical Supercapacitors: Scientific Fundamentals and Technological Applications*; Kluwer Academic/Plenum: New York, 1999.
12. Bélanger, D.; Brousse, T.; Long, J. W. Manganese Oxides: Battery Materials Make the Leap to Electrochemical Capacitors. *Electrochem. Soc. Interface* **2008**, 49–52.
13. Wei, W. F.; Cui, X. W.; Chen, W. X.; Ivey, D. G. Manganese Oxide-Based Materials as Electrochemical Supercapacitor Electrodes. *Chem. Soc. Rev.* **2011**, *40*, 1697–1721.
14. Ghaemi, M.; Ataherian, F.; Zolfaghari, A.; Jafari, S. M. Charge Storage Mechanism of Sonochemically Prepared MnO_2 as Supercapacitor Electrode: Effects of Physisorbed Water

and Proton Conduction. *Electrochim. Acta* **2008**, *53*, 4607–4614.

15. Yan, J.; Fan, Z. J.; Wei, T.; Qian, W. Z.; Zhang, M. L.; Wei, F. Fast and Reversible Surface Redox Reaction of Graphene−MnO₂ Composites as Supercapacitor Electrodes. *Carbon* **2010**, *48*, 3825–3833.

16. Brousse, T.; Taberna, P.-L.; Crosnier, O.; Dugas, R.; Guillemet, P.; Scudeller, Y.; Zhou, Y.; Favier, F.; Bélanger, D.; Simon, P. Long-Term Cycling Behavior of Asymmetric Activated Carbon/MnO₂ Aqueous Electrochemical Supercapacitor. *J. Power Sources* **2007**, *173*, 633–641.

17. Reddy, A. L. M.; Shaijumon, M. M.; Gowda, S. R.; Ajayan, P. M. Multisegmented Au-MnO₂/Carbon Nanotube Hybrid Coaxial Arrays for High-Power Supercapacitor Applications. *J. Phys. Chem. C* **2009**, *114*, 658–663.

18. Rakhi, R. B.; Cha, D.; Chen, W.; Alshareef, H. N. Electrochemical Energy Storage Devices Using Electrodes Incorporating Carbon Nanocoils and Metal Oxides Nanoparticles. *J. Phys. Chem. C* **2011**, *115*, 14392–14399.

19. Sivakkumar, S. R.; Ko, J. M.; Kim, D. Y.; Kim, B. C.; Wallace, G. G. Performance Evaluation of CNT/Polypyrrole/MnO₂ Composite Electrodes for Electrochemical Capacitors. *Electrochim. Acta* **2007**, *52*, 7377–7385.

20. Ma, S. B.; Nam, K. W.; Yoon, W. S.; Yang, X. Q.; Ahn, K. Y.; Oh, K. H.; Kim, K. B. Electrochemical Properties of Manganese Oxide Coated onto Carbon Nanotubes for Energy-Storage Applications. *J. Power Sources* **2008**, *178*, 483–489.

21. Wu, Z. S.; Ren, W. C.; Wang, D. W.; Li, F.; Liu, B. L.; Cheng, H. M. High-Energy MnO₂ Nanowire/Graphene and Graphene Asymmetric Electrochemical Capacitors. *ACS Nano* **2010**, *4*, 5835–5842.

22. Chen, S.; Zhu, J. W.; Wu, X. D.; Han, Q. F.; Wang, X. Graphene Oxide−MnO₂ Nanocomposites for Supercapacitors. *ACS Nano* **2010**, *4*, 2822–2830.

23. Reddy, A. L. M.; Shaijumon, M. M.; Gowda, S. R.; Ajayan, P. M. Coaxial MnO₂/Carbon Nanotube Array Electrodes for High-Performance Lithium Batteries. *Nano Lett.* **2009**, *9*, 1002–1006.

24. Hou, Y.; Cheng, Y. W.; Hobson, T.; Liu, J. Design and Synthesis of Hierarchical MnO₂ Nanospheres/Carbon Nanotubes/Conducting Polymer Ternary Composite for High Performance Electrochemical Electrodes. *Nano Lett.* **2010**, *10*, 2727–2733.

25. Lee, S. W.; Kim, J.; Chen, S.; Hammond, P. T.; Shao-Horn, Y. Carbon Nanotube/Manganese Oxide Ultrathin Film Electrodes for Electrochemical Capacitors. *ACS Nano* **2010**, *4*, 3889–3896.

26. Lang, X.; Hirata, A.; Fujita, T.; Chen, M. Nanoporous Metal/Oxide Hybrid Electrodes for Electrochemical Supercapacitors. *Nat. Nanotechnol.* **2011**, *6*, 232–236.

27. Hu, L. B.; Choi, J. W.; Yang, Y.; Jeong, S.; La Mantia, F.; Cui, L. F.; Cui, Y. Highly Conductive Paper for Energy-Storage Devices. *Proc. Natl. Acad. Sci. U.S.A.* **2009**, *106*, 21490–21494.

28. Hu, L. B.; Pasta, M.; La Mantia, F.; Cui, L. F.; Jeong, S.; Deshazer, H. D.; Choi, J. W.; Han, S. M.; Cui, Y. Stretchable, Porous, and Conductive Energy Textiles. *Nano Lett.* **2010**, *10*, 708–714.

29. Kang, Y. J.; Kim, B.; Chung, H.; Kim, W. Fabrication and Characterization of Flexible and High Capacitance Supercapacitors Based on MnO₂/CNT/Papers. *Synth. Met.* **2010**, *160*, 2510–2514.

30. Fischer, A. E.; Pettigrew, K. A.; Rolison, D. R.; Stroud, R. M.; Long, J. W. Incorporation of Homogeneous, Nanoscale MnO₂ within Ultraporous Carbon Structures *via* Self-Limiting Electroless Deposition: Implications for Electrochemical Capacitors. *Nano Lett.* **2007**, *7*, 281–286.

31. Lytle, J. C.; Wallace, J. M.; Sassin, M. B.; Barrow, A. J.; Long, J. W.; Dysart, J. L.; Renninger, C. H.; Saunders, M. P.; Brandell, N. L.; Rolison, D. R. The Right Kind of Interior for Multifunctional Electrode Architectures: Carbon Nanofoam Papers with Aperiodic Submicrometre Pore Networks Interconnected in 3D. *Energy Environ. Sci.* **2011**, *4*, 1913–1925.

32. Zhang, G. X.; Sun, S. H.; Yang, D. Q.; Dodelet, J. P.; Sacher, E. The Surface Analytical Characterization of Carbon Fibers Functionalized by H₂SO₄/HNO₃ Treatment. *Carbon* **2008**, *46*, 196–205.

33. Stoller, M. D.; Ruoff, R. S. Best Practice Methods for Determining an Electrode Material's Performance for Ultracapacitors. *Energy Environ. Sci.* **2010**, *3*, 1294–1301.

34. Toupin, M.; Brousse, T.; Belanger, D. Charge Storage Mechanism of MnO₂ Electrode Used in Aqueous Electrochemical Capacitor. *Chem. Mater.* **2004**, *16*, 3184–3190.

35. Cottineau, T.; Toupin, M.; Delahaye, T.; Brousse, T.; Belanger, D. Nanostructured Transition Metal Oxides for Aqueous Hybrid Electrochemical Supercapacitors. *Appl. Phys. A* **2006**, *82*, 599–606.

36. Chen, P. C.; Shen, G. Z.; Shi, Y.; Chen, H. T.; Zhou, C. W. Preparation and Characterization of Flexible Asymmetric Supercapacitors Based on Transition-Metal-Oxide Nanowire/Single-Walled Carbon Nanotube Hybrid Thin-Film Electrodes. *ACS Nano* **2010**, *4*, 4403–4411.

37. Hsieh, Y.-C.; Lee, K.-T.; Lin, Y.-P.; Wu, N.-L.; Donne, S. W. Investigation on Capacity Fading of Aqueous MnO₂·nH₂O Electrochemical Capacitor. *J. Power Sources* **2008**, *177*, 660–664.